Space Weather

RESEARCH ARTICLE
10.1029/2018SW001969

Special Section:
Space Weather Events of 4-10 September 2017

The 6 September 2017 X9 Super Flare Observed From Submillimeter to Mid-IR

C. G. Giménez de Castro[1,2], J.-P. Raulin[1], J. F. Valle Silva[1], P. J. A. Simões[3], A. S. Kudaka[1], and A. Valio[1]

[1]Centro de Rádio Astronomia e Astrofísica Mackenzie, Escola de Engenharia, Universidade Presbiteriana Mackenzie, São Paulo, Brazil, [2]Instituto de Astronomía y Física del Espacio, CONICET, Buenos Aires, Argentina, [3]SUPA School of Physics and Astronomy, University of Glasgow, Glasgow, UK

Key Points:
- SOL2017-09-06T12:00 is the most intense flare of cycle 24
- The IR emission has a similar time evolution as the white light and very different from the microwaves at 15.4 GHz
- The radio emission at 212 and 405 GHz comes from a different source than the microwaves

Correspondence to:
C. G. Giménez de Castro,
guigue@craam.mackenzie.br

Citation:
Gimenez de Castro, C. G., Raulin, J.-P., Valle Silva, J. F., Simões, P. J. A., Kudaka, A. S., & Valio, A. (2018). The 6 September 2017 X9 super flare observed from submillimeter to mid-IR. *Space Weather*, *16*, 1261–1268. https://doi.org/10.1029/2018SW001969

Received 30 MAY 2018
Accepted 26 JUL 2018
Accepted article online 11 AUG 2018
Published online 6 SEP 2018

Abstract Active Region 12673 is the most productive active region of solar cycle 24: in a few days of early September 2017, four X-class and 27 M-class flares occurred. SOL2017-09-06T12:00, an X9.3 flare also produced a two-ribbon white light emission across the sunspot detected by Solar Dynamics Orbiter/Helioseismic and Magnetic Imager. The flare was observed at 212 and 405 GHz with the arcminute-sized beams of the Solar Submillimeter Telescope focal array while making a solar map and at 10 μm, with a 17 arcsec diffraction-limited infrared camera. Images at 10 μm revealed that the sunspot gradually increased in brightness while the event proceeded, reaching a temperature similar to quiet Sun values. From the images we derive a lower bound limit of 180-K flare peak excess brightness temperature or 7,000 sfu if we consider a similar size as the white light source. The rising phase of mid-IR and white light is similar, although the latter decays faster, and the maximum of the mid-IR and white light emission is ∼ 200 s delayed from the 15.4-GHz peak occurrence. The submillimeter spectrum has a different origin than that of microwaves from 1 to 15 GHz, although it is not possible to draw a definitive conclusion about its emitting mechanism.

1. Introduction

Solar flares in the mid-infrared (IR) domain have been detected only recently. The first observation at 10 μm (30 THz) was reported by Kaufmann et al. (2013) for the Geostationary Operational Environmental Satellite (GOES) M2 event SOL2012-03-13T17:20, which also exhibited white light (WL) emission with a remarkable coincidence both in space and in time. Trottet et al. (2015) interpret the mid-IR emission as optically thin thermal from the chromosphere heated by precipitating electrons and ions. Penn et al. (2016) observed the C7 event SOL2014-09-24T17:50 with two cameras with filters centered at 5.2 and 8.2 μm (57.7 and 36.6 THz, respectively) and high spatial resolution. Two mid-IR sources were observed to be cospatial with WL and hard X-ray foot points. The flux at both wavelengths is of the same order, lending support to a thermal optically thin origin, a conclusion further reinforced by results of radiative hydrodynamic simulations by Simões et al. (2017). Two other events were registered at 10 μm: SOL2014-08-01T14:47 (Miteva et al., 2016) and SOL2014-10-27T14:22 (Kaufmann et al., 2015), the last one classified as X2.

Emission at submillimeter frequencies during flares is being routinely observed since 2001 when the Solar Submillimeter Telescope (SST; Kaufmann, et al., 2008) started daily operations at 0.7 (405 GHz) and 1.4 mm (212 GHz). The origin of the submillimeter emission during the impulsive phase of a flare is still controversial. In some cases it was found that it is mostly optically thin gyrosynchrotron emission produced by greater than megaelectron volts electrons (Cristiani et al., 2007; Giménez de Castro et al., 2009; Raulin et al., 2004; Trottet et al., 2002). Some other events present a positive slope between 212 and 405 GHz different from the microwave source that was interpreted as optically thick gyrosynchrotron emission from a second source inside a strong magnetic field and with a much smaller size (Kaufmann et al., 2009; Silva et al., 2007). Nonetheless, other emitting mechanisms cannot be ruled out since the spectral coverage is still very much incomplete. Krucker et al. (2013) give a comprehensive and critical analysis of all possible processes that may be responsible for the submillimeter emission. On the other hand, the extended or gradual phase of flares can be attributed to thermal bremsstrahlung (Lüthi, Lüdi, & Magun, 2004; Lüthi, Magun, & Miller, 2004; Trottet et al., 2002, 2011).

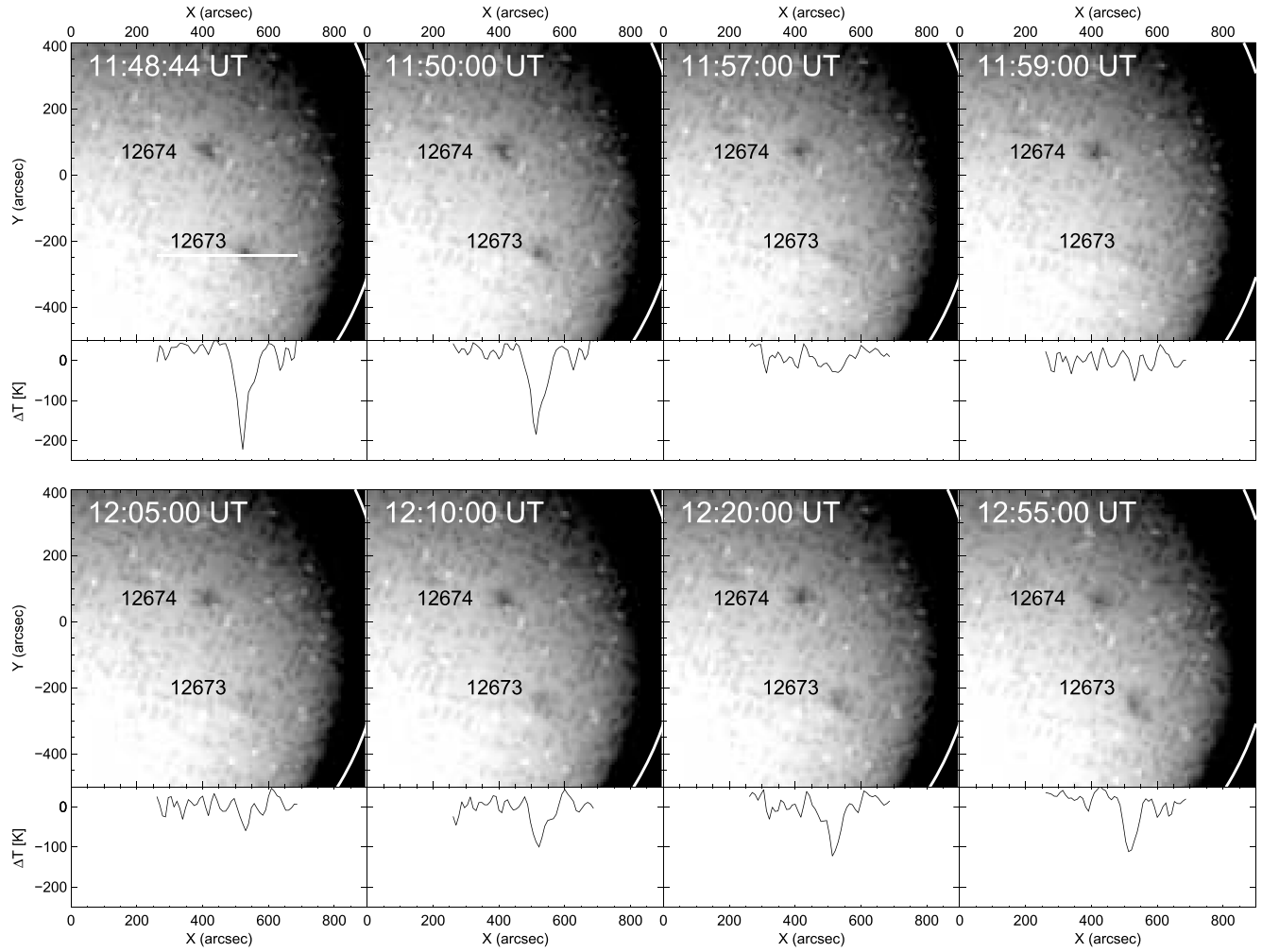

Figure 1. Time evolution of the spot associated to AR 12673 during the flare observed at 10 μm. While the flare progresses, the spot becomes less dark until it is indistinguishable from the quiet Sun; as a reference we show the spot associated to AR 12674 in the north. Below every image we plot a slice in the *X* direction with the intensity over the flaring spot relative to quiet Sun. The location where the slices are taken is shown in the first panel with a white line.

The unexpected and intense activity of the active region (AR) numbered 12673 by the National Oceanic and Atmospheric Administration (NOAA) led many researchers to describe it as a *Super Active Region* (see Romano, et al., 2018). Indeed, the region, which was in a decaying phase, experienced new flux emergence and produced between 4 and 10 September 2017 tens of GOES C-class, 27 M-class, and 4 X-class flares as a result of the greatest magnetic flux emergence ever observed (Sun & Norton, 2017). On 6 September, it produced two X-class flares: the X2.2 SOL2017-09-06T08:57 and the X9.3 SOL2017-09-06T11:53 (hereafter SOL2017-09-06), the most powerful event of cycle 24. These events are peculiar not only because of their soft X-ray flux but also because they produced WL emission, being a rare case of homologous WL flares (Romano et al., 2018). Moreover, SOL2017-09-06 produced two coronal mass ejections, one near the peak time and the next 1 hr later (Goryaev et al., 2018). It was pointed out that the total emitted energy by the flare is about $10^{(25)}$ J, that is, in the lower limit of a *super flare* (Kolotkov et al., 2018). In this paper we report the observation of SOL2017-09-06 at the wavelengths of 10 μm (mid-IR) and 0.7 and 1.4 mm (submillimeter).

2. Mid-Infrared Observations

Observations at $\lambda = 10$ μm ($\nu = 30$ THz) were carried out with the São Paulo 30-THz telescope (SP30T; Kudaka et al., 2015) which is a Newtonian system with a 15-cm aperture, resulting in a diffraction limit $\vartheta_d \simeq 17''$. The original setup described in Kudaka et al. (2015) was changed to have now a FLIR TermoVision™ A20 M camera with a Focal Plane Array uncooled microbolometer of 160 × 120 pixels that produces interpolated

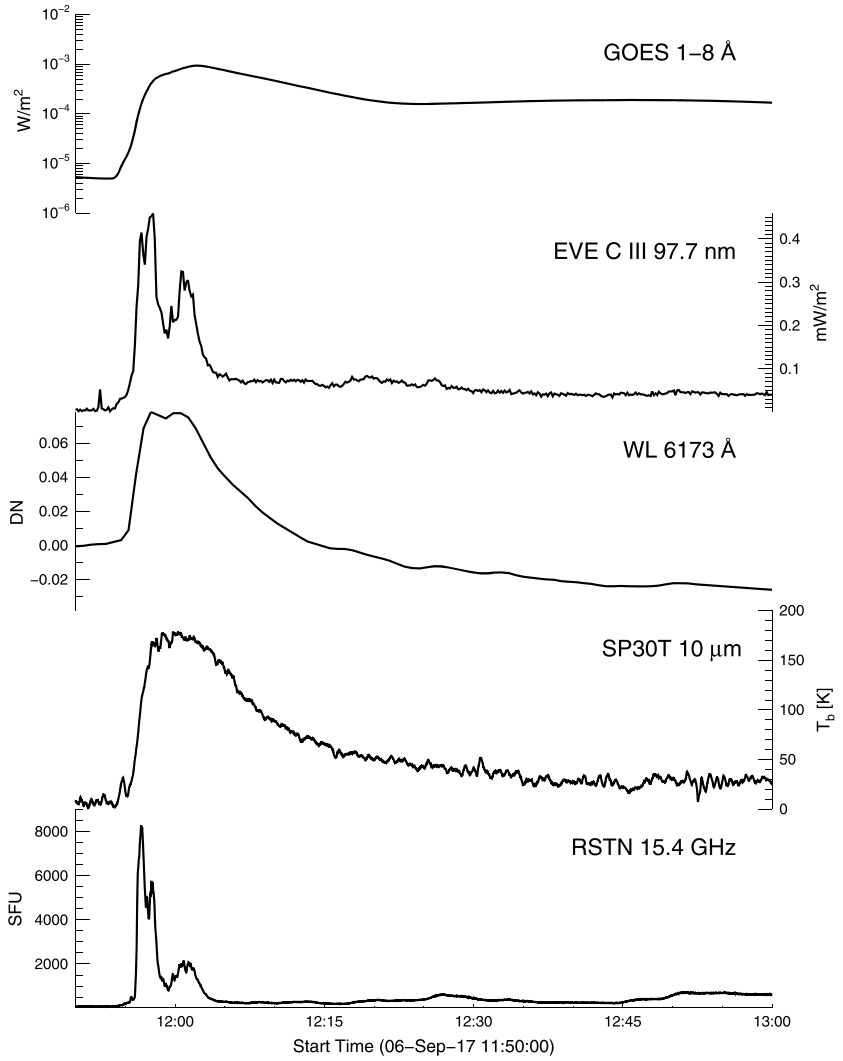

Figure 2. Intensity time profiles at selected wavelengths. GOES = Geostationary Operational Environmental Satellite; EVE = Extreme Ultraviolet Variability Experiment; WL = white light; RSTN = Radio Solar Telescope Network.

digital frames of 320 × 240 pixels with a temperature accuracy ±2 °C (internal calibration) or ±2%. The optical setup ensures that the real pixels have the same size as ϑ_d.

On the morning of 6 September 2017, São Paulo had a clear sky, excellent for observations even at large zenith distance. Observations started at around 8:30 local time (11:30 UTC) and lasted past local noon (15:00 UTC), producing movies with 10 min duration at one frame per second. Every frame was exported to FITS format to be able to manipulate it with nonproprietary software. Although the camera has internal procedures that calibrate in temperature, we applied an external calibration against the Sun. Every image was rescaled to have a quiet Sun excess temperature over the sky $T_b = 5000$ K (Turon & Léna, 1970); in this way we removed any possible influence from the terrestrial atmosphere and the optical system. Two spots were visible on the solar disc: one in the Northern Hemisphere inside AR 12674 and the other in the Southern Hemisphere, within the flaring AR 12673. Figure 1 displays frames at different moments of the event. Below every image is shown a slice in the *X* direction crossing the center of the flaring region spot. Since the camera could not spatially resolve the emitting region no actual peak in intensity is observed, but rather the images show that, as the flare evolves, the spot becomes less dark, until it is as bright as the surrounding quiet Sun, at around 11:59:00 UT. Afterward, the dark spot reappears gradually. To extract the time profile, we used a 2-D *à Trous* wavelet decomposition, based on a triangle mother wavelet (Starck & Murtagh, 2006), to reduce random pixel fluctuations. We fitted a 2-D Gaussian to the square of the third scale of the wavelet transform matrix of each frame. The square root of the amplitude of the 2-D Gaussian was preflare subtracted. At the end, one still has to rescale the obtained

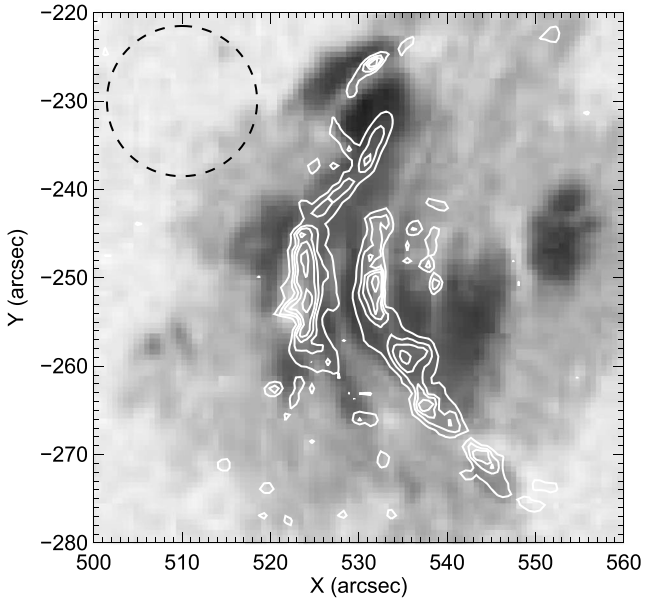

Figure 3. An SDO/HMI 6,173 Å image taken at 11:40:00 UT, just before the flare. Overplotted, contours at levels $\{5,\ 8,\ 10,\ 12,\ 15\} \times 10^3$ DN above preflare values of the WL emission during peak time (12:00:34 UT). The dashed circle in the top left corner represents the Airy disk of the SP30T camera. SDO = Solar Dynamics Orbiter; HMI = Helioseismic and Magnetic Imager.

temperatures since the wavelet decomposition gives a weighted mean of the area. To do this, the first frame, where the spot is sharply defined, was fitted to a 2-D Gaussian: the ratio between Gaussian amplitude and the one obtained with the wavelet transform was used to rescale the whole time series.

The final time profile after being filtered with a 10-s running mean is illustrated in Figure 2, where other wavelengths are also shown: soft X-rays from the GOES 1–8 Å, C III 97.7 nm from the Extreme Ultraviolet Variability Experiment (EVE, Woods, et al., 2012) onboard the Solar Dynamics Orbiter (SDO), the spatially integrated contrast $(F_f - F_0)/F_0$ of the continuum at 6,173 Å obtained from the Helioseismic and Magnetic Imager (HMI) onboard the SDO and microwaves at 15.4 GHz from the Radio Solar Telescope Network (RSTN). Figure 3 shows an image of the region before the flare started in the continuum 6,173 Å; overplotted, the white contours represent the two-ribbon WL emission at peak time (12:00:34 UT). From the image we can infer a WL emitting area $A_{wl} \sim 3 \times 10^{18}$ cm^2. The WL excess contours were obtained as follows: the series of HMI I_c images were processed with the standard routine (aia_prep) and co-aligned using the routine drot_map in the SolarSoft

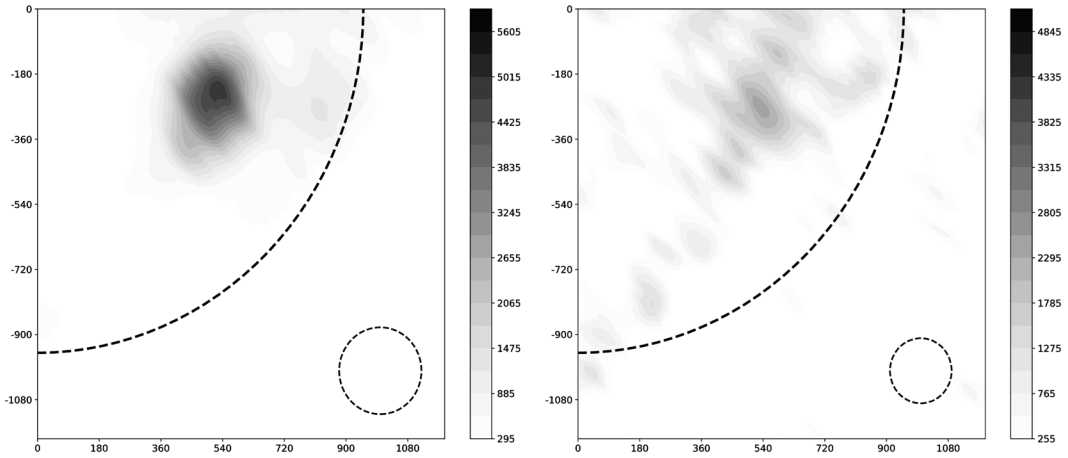

Figure 4. Solar Submillimeter Telescope maps starting at 11:53 UT: left panel is for 212 GHz, and right panel is for 405 GHz. The dashed circles in the bottom right corner represent the beams Half Power Beam Width (HPBW).

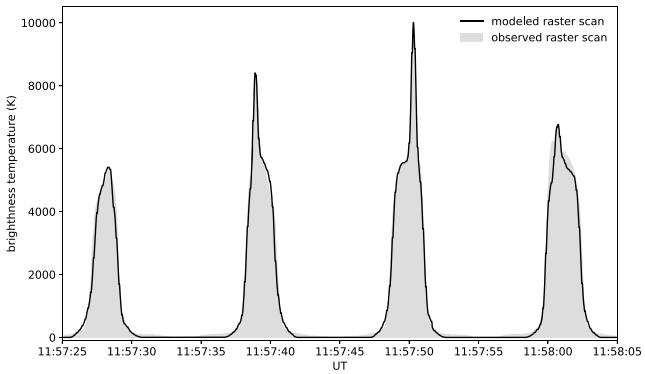

Figure 5. Observed (gray) and modeled (black) raster scan profiles. Scans are in azimuth with a fixed elevation. After each scan, the elevation is changed and the movement direction in azimuth is reversed, that is, after an east to west follows a west to east movement. Then, again east to west, etc.

(SSW, see http://www.lmsal.com/solarsoft) package; a mean preflare image (between 11:40 to 11:50 UT) was obtained and then subtracted from the image taken near the maximum of the impulsive phase (12:00:34 UT).

3. The Submillimeter Emission

At 11:53 UT the Solar Submillimeter Telescope started a solar map. It took 11 min to complete, including the whole impulsive phase. Figure 4 displays calibrated maps at 212 and 405 GHz, obtained through raster scans. Between 11:56:30 and 11:58:00 UT, the bursting area was unresolved, that is, it remained within the e^{-2} width region of the beams. Maps are calibrated against the quiet Sun, adopting a brightness temperature 5900 and 5100 K for 212 and 405 GHz, respectively (Silva et al., 2005).

In order to determine the average value of flux density over the period of 90 s beginning at 11:56:30 UT, maps were synthesized adopting for the quiet Sun a disk plus another disk for the flaring source; these were convolved with the beams' matrix representation. Two different values for the emitting source size were considered: (i) a compact 25″, which is in accord with what Lüthi et al. (2004) determined as the average 210-GHz source during the impulsive phase of SOL2003-10-28 and also in agreement with the WL area of our event, and (2) an extended 120″ covering the entire AR 12673. For each case, excess brightness temperatures over the emitting source were determined fitting the observed raster scans. Figure 5 shows the observed and modeled raster scans recovered with one of the four 212-GHz beams. Although the brightness temperatures are very different for the two assumed source sizes, the flux densities are similar, with differences attributable to uncertainties in the fitting procedure.

The process must be repeated for each of the beams observing at the same frequency (four at 212 GHz and two at 405 GHz) until recovering compatible flux density time profiles. To fit the 405-GHz raster scans, it was necessary to consider a smaller temperature. The fitting accuracy was poorer at 405 GHz as a consequence of the increased noise in the maps. Final results for the modeling are shown in Table 1.

4. Discussion

To compare the light curves, the normalized fluxes are plotted together in Figure 6. It can be seen that the WL and mid-IR start and peak together, although the former cools faster. Microwave emissions start together with these two wavelengths but peak before and have an impulsive shape with short pulses until 12:05 UT.

Table 1
Model Parameters and Results

Frequency (GHz)	Source size (″)	Excess temperature (MK)	Flux (sfu)
212	25	1.75 ± 0.11	$2,900 \pm 250$
405	25	0.58 ± 0.42	$4,800 \pm 1,400$
212	120	0.09 ± 0.01	$3,300 \pm 300$
405	120	0.03 ± 0.03	$4,300 \pm 1,800$

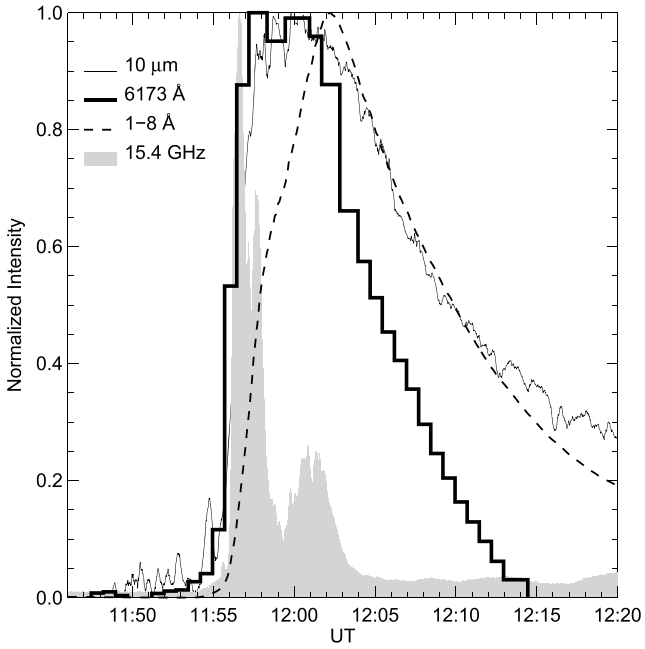

Figure 6. Normalized time profiles at selected wavelengths. UT = universal time.

Afterward, the intensity remains at 5% level with respect to the maximum, which can be an indication of thermal emission. Soft X-rays start almost together with the rest but increase slower, having the peak flux later. After the peak, it drops at a similar pace with the mid-IR during the time interval shown. The brightness temperature at 10 μm (Figure 2) should be considered as a lower bound value since the spatial resolution of our camera is of the same order of the emitting source size. Assuming that the mid-IR source is cospatial with the WL source, as it was observed by Penn et al. (2016) with higher spatial resolution; the intensity we observe at 10 μm might be an average of dark and bright areas (see Figure 3). Indeed, we do not see a brightening but only variations in the darkness of the spot (Figure 1). Adopting the WL emitting area for the mid-IR source size, we obtain a peak flux of $F_{10\mu m} \geq 7,000$ sfu.

In Figure 7 we show the radio spectrum resulting for a compact submillimeter emitting source, along with microwaves observed by the San Vito RSTN station, and the lower bound limit for the mid-IR. From the spectrum at peak time we cannot determine the gyrosynchrotron turnover frequency at microwaves. On the other hand, the submillimeter emission seems to come from a different emitting mechanism because (i) the flux density is an average during the impulsive phase where we adopted a constant brightness temperature, that is, the instantaneous peak flux density must be much higher than what we have determined and, probably, higher than the 15.4-GHz flux density and (ii) flux at 212 is smaller than that at 405 GHz (or, in the limit of the error bar, of the same order). From the results of our models (see Table 1) we note that the flux is weakly dependent on the adopted source size. However, it is not possible to determine whether the submillimeter emission comes from a nonthermal source or not; if thermal, however, each frequency would form at different plasma temperatures, that is, a multithermal source is required. In this latter case, a similar result for the extended phase of SOL2003-10-27 was found by Trottet et al. (2011) who modeled the emission in the range 8–230 GHz with a multithermal greater than megakelvin optically thin source. They also observed that 345 GHz is optically thick and should come from a lower height. In our case, if the emission were optically thick gyrosynchrotron, the spectral index between 212 and 405 GHz, $\alpha \simeq 0.8$, would indicate an inhomogeneous source (Klein & Trottet, 1984; Simões & Costa, 2006), while Tsap et al. (2018) propose a mixture of gyrosynchrotron and thermal bremsstrahlung absorption to explain the spectral increase between 93 and 140 GHz during SOL2012-07-05T11:44. The mid-IR flux can be explained, as in Trottet et al. (2015), as optically thin thermal bremsstrahlung emission of a heated chromospheric plasma, since fluxes of the two events are similar. Moreover, Simões et al. (2017), using radiative hydrodynamic simulations, have demonstrated that the mid-IR emission from solar flares may be accounted by optically thin thermal bremsstrahlung due to the increase of the electron density in the chromosphere, as a consequence of the ionization of hydrogen under non local thermodynamical equilibrium (non-LTE) conditions.

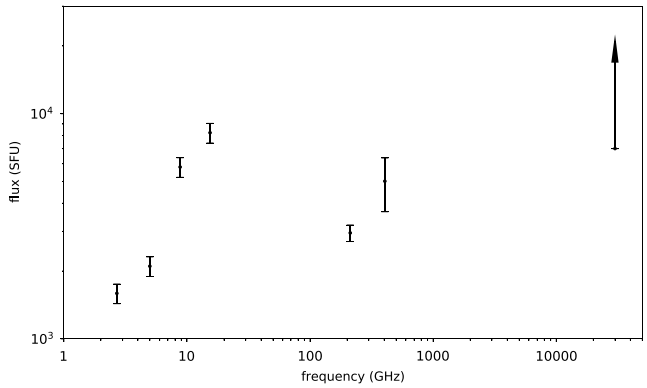

Figure 7. Spectrum of the flare, from microwaves to midinfrafed, at peak time 11:56:46 UT. SFU = solar flux unit.

Super flares as the one studied in this paper bring new clues to better understand different aspects of space weather dynamics and perhaps the most relevant, that is, the origin of solar flares. The high-frequency spectrum of solar flares, and its connection with the flaring infrared emission, is still a very new aspect of solar flare studies. This relation may also reveal the nature of the WL emission for which we do not have a clear explanation at the present time. Finally, these events sometimes present an unusual behavior as diagnosed at few hundreds of gigahertz, which may indicate the presence of ultrarelativistic electrons and protons that travel through the interplanetary medium, reach the Earth's orbit, and penetrate its atmosphere. However, observations at submillimeter to mid-IR frequencies are scarce, and many frequency gaps must be filled. The Atacama Large Millimeter Array and the Large Latin American Millimeter Array will widen the submillimeter range up to 900 GHz. The High-Altitude THz Solar telescope, with first light expected in 2020, will observe the unexplored wavelength of 20 μm. Moreover, a spaceborne Solar-T (Kaufmann et al., 2016), observing at 100 and 43 μm, is expected to fly during the new cycle 25.

To summarize our findings, our observations endorse the similarities between the light curves at mid-IR frequencies and WL previously reported (Kaufmann et al., 2013, 2015; Miteva et al., 2016; Penn et al., 2016), although these emissions have different origins. Another important result is that the derived flux at mid-IR is well above the obtained density flux at submillimeter wavelengths and detected even with a commercial camera in the focus of a small telescope. We finally note that the long duration (more than 1 hr) of the 10-μm emission remains as an open question.

Acknowledgments
This research was financed by the Brazilian Agency FAPESP through grant 2013/24155-3, by the U.S. Air Force Office for Scientific Research FA9550-16-1-0072, and by the MackPesquisa grant. P. J. A. S. acknowledges support from the University of Glasgow's Lord Kelvin Adam Smith Leadership Fellowship. C. G. G. C. and J. P. R. are thankful to CNPq by the support through grants 305203/2016-9 and 312066/2016-3, respectively. Data used in this research are public and can be downloaded from `https://github.com/guigue/SOL20170906/`. Please read the wiki for more information on how to reduce the data.

References

Cristiani, G., Martinez, G., Mandrini, C. H., Giménez de Castro, C. G., da Silva, C. W., Rovira, M. G., & Kaufmann, P. (2007). Spatial characterization of a flare using radio observations and magnetic field topology. *Solar Physics*, *240*, 271–281. https://doi.org/10.1007/s11207-006-0337-5

Giménez de Castro, C. G., Trottet, G., Silva-Valio, A., Krucker, S., Costa, J. E. R., Kaufmann, P., et al. (2009). Submillimeter and X-ray observations of an X class flare. *Astronomy & Astrophysics*, *507*, 433–439. https://doi.org/10.1051/0004-6361/200912028

Goryaev, F. F., Slemzin, V. A., Rodkin, D. G., D'Huys, E., Podladchikova, O., & West, M. J. (2018). Brightening and darkening of the extended solar corona during the superflares of September 2017. *Astrophysical Journal*, *856*, L38. https://doi.org/10.3847/2041-8213/aab849

Kaufmann, P., Abrantes, A., Bortolucci, E., Caspi, A., Fernandes, L. O. T., Kropotov, G., et al. (2016). Solar observations at THz frequencies on board of a trans-Antartic stratospheric balloon flight. *AAS/Solar Physics Division Meeting*, *47*, 11.

Kaufmann, P., Levato, H., Cassiano, M. M., Correia, E., Costa, J. E. R., Giménez de Castro, C. G., et al. (2008). New telescopes for ground-based solar observations at submillimeter and mid-infrared. *Ground-based and Airborne Telescopes II*, *7012*, 70120L. https://doi.org/10.1117/12.788889

Kaufmann, P., Raulin, J.-P., de Castro, C. G. G., Levato, H., Gary, D. E., Costa, J. E. R., et al. (2004). A new solar burst spectral component emitting only in the terahertz range. *Astrophysical Journal*, *603*, L121. https://doi.org/10.1086/383186

Kaufmann, P., Trottet, G., Giménez de Castro, C. G., Raulin, J.-P., Krucker, S., Shih, A. Y., & Levato, H. (2009). Sub-terahertz, microwaves and high energy emissions during the 6 December 2006 flare, at 18:40 UT. *Solar Physics*, *255*, 131–142. https://doi.org/10.1007/s11207-008-9312-7

Kaufmann, P., White, S. M., Freeland, S. L., Marcon, R., Fernandes, L. O. T., Kudaka, A. S., et al. (2013). A bright impulsive solar burst detected at 30 THz. *Astrophysical Journal*, *768*, 134. https://doi.org/10.1088/0004-637X/768/2/134

Kaufmann, P., White, S. M., Marcon, R., Kudaka, A. S., Cabezas, D. P., Cassiano, M. M., et al. (2015). Bright 30 THz impulsive solar bursts. *Journal of Geophysical Research: Space Physics*, *120*, 4155–4163. https://doi.org/10.1002/2015JA021313

Klein, K.-L., & Trottet, G. (1984). Gyrosynchrotron radiation from a source with spatially varying field and density. *Astronomy & Astrophysics*, *141*, 67–76.

Kolotkov, D. Y., Pugh, C. E., Broomhall, A.-M., & Nakariakov, V. M. (2018). Quasi-periodic pulsations in the most powerful solar flare of cycle 24. *Astrophysical Journal*, *858*, L3. https://doi.org/10.3847/2041-8213/aabde9

Krucker, S., Giménez de Castro, C. G., Hudson, H. S., Trottet, G., Bastian, T. S., Hales, A. S., et al. (2013). Solar flares at submillimeter wavelengths. *Astronomy and Astrophysics Review*, *21*, 58. https://doi.org/10.1007/s00159-013-0058-3

Kudaka, A. S., Cassiano, M. M., Marcon, R., Cabezas, D. P., Fernandes, L. O. T., Ramirez, H., et al. (2015). The new 30 THz solar telescope in são Paulo, Brazil. *Solar Physics*, *290*, 2373–2379. https://doi.org/10.1007/s11207-015-0749-1

Lüthi, T., Lüdi, A., & Magun, A. (2004). Determination of the location and effective angular size of solar flares with a 210 GHz multibeam radiometer. *Astronomy & Astrophysics*, *420*, 361–370. https://doi.org/10.1051/0004-6361:20035899

Lüthi, T., Magun, A., & Miller, M. (2004). First observation of a solar X-class flare in the submillimeter range with KOSMA. *Astronomy & Astrophysics*, *415*, 1123–1132. https://doi.org/10.1051/0004-6361:20034624

Miteva, R., Kaufmann, P., Cabezas, D. P., Cassiano, M. M., Fernandes, L. O. T., Freeland, S. L., et al. (2016). Comparison of 30 THz impulsive burst time development to microwaves, Hα, EUV, and GOES soft X-rays. *Astronomy & Astrophysics*, *586*, A91. https://doi.org/10.1051/0004-6361/201425520

Penn, M., Krucker, S., Hudson, H., Jhabvala, M., Jennings, D., Lunsford, A., & Kaufmann, P. (2016). Spectral and imaging observations of a white-light solar flare in the mid-infrared. *Astrophysical Journal*, *819*, L30. https://doi.org/10.3847/2041-8205/819/2/L30

Raulin, J. P., Makhmutov, V. S., Kaufmann, P., Pacini, A. A., Lüthi, T., Hudson, H. S., & Gary, D. E. (2004). Analysis of the impulsive phase of a solar flare at submillimeter wavelengths. *Solar Physics*, *223*, 181–199. https://doi.org/10.1007/s11207-004-1300-y

Romano, P., Elmhamdi, A., Falco, M., Costa, P., Kordi, A. S., Al-Trabulsy, H. A., & Al-Shammari, R. M. (2018). Homologous white light solar flares driven by photospheric shear motions. *Astrophysical Journal*, *852*, L10. https://doi.org/10.3847/2041-8213/aaa1df

Silva, A. V. R., Laganá, T. F., Gimenez Castro, C. G., Kaufmann, P., Costa, J. E. R., Levato, H., & Rovira, M. (2005). Diffuse component spectra of solar active regions at submillimeter wavelengths. *Solar Physics*, *227*, 265–281. https://doi.org/10.1007/s11207-005-2787-6

Silva, A. V. R., Share, G. H., Murphy, R. J., Costa, J. E. R., de Castro, C. G. G., Raulin, J.-P., & Kaufmann, P. (2007). Evidence that synchrotron emission from nonthermal electrons produces the increasing submillimeter spectral component in solar flares. *Solar Physics*, *245*, 311–326. https://doi.org/10.1007/s11207-007-9044-0

Simões, P. J. A., Kerr, G. S., Fletcher, L., Hudson, H. S., Giménez de Castro, C. G., & Penn, M. (2017). Formation of the thermal infrared continuum in solar flares. *Astronomy & Astrophysics*, *605*, A125. https://doi.org/10.1051/0004-6361/201730856

Simões, P. J. A., & Costa, J. E. R. (2006). Solar bursts gyrosynchrotron emission from three-dimensional sources. *Astronomy & Astrophysics*, *453*, 729–736. https://doi.org/10.1051/0004-6361:20054665

Starck, J.-L., & Murtagh, F. (2006). *Astronomical image and data analysis*. Berlin Heidelberg: Springer Verlag. https://doi.org/10.1007/978-3-540-33025-7

Sun, X., & Norton, A. A. (2017). Super-flaring active region 12673 has one of the fastest magnetic flux emergence ever observed. *Research Notes of the American Astronomical Society*, *1*, 24. https://doi.org/10.3847/2515-5172/aa9be9

Trottet, G., Raulin, J.-P., Giménez de Castro, G., Lüthi, T., Caspi, A., Mandrini, C. H., et al. (2011). Origin Of the submillimeter radio emission during the time-extended phase of a solar flare. *Solar Physics*, *273*, 339–361. https://doi.org/10.1007/s11207-011-9875-6

Trottet, G., Raulin, J.-P., Kaufmann, P., Siarkowski, M., Klein, K.-L., & Gary, D. E. (2002). First detection of the impulsive and extended phases of a solar radio burst above 200 GHz. *Astronomy & Astrophysics*, *381*, 694–702. https://doi.org/10.1051/0004-6361:20011556

Trottet, G., Raulin, J.-P., Mackinnon, A., Giménez de Castro, G., Simões, P. J. A., Cabezas, D., et al. (2015). Origin of the 30 THz emission detected during the solar flare on 2012 March 13 at 17:20 UT. *Solar Physics*, *290*, 2809–2826. https://doi.org/10.1007/s11207-015-0782-0

Tsap, Y. T., Smirnova, V. V., Motorina, G. G., Morgachev, A. S., Kuznetsov, S. A., Nagnibeda, V. G., & Ryzhov, V. S. (2018). Millimeter and X-Ray emission from the 5 July 2012 solar flare. *Solar Physics*, *293*, 50. https://doi.org/10.1007/s11207-018-1269-6

Turon, P. J., & Léna, P. J. (1970). High resolution solar images at 10 microns: Sunspot details and photometry. *Solar Physics*, *14*, 112–124. https://doi.org/10.1007/BF00240164

Woods, T. N., Eparvier, F. G., Hock, R., Jones, A. R., Woodraska, D., Judge, D., et al. (2012). Extreme ultraviolet variability experiment (EVE) on the solar dynamics observatory (SDO): Overview of science objectives, instrument design, data products, and model developments. *Solar Physics*, *275*, 115–143. https://doi.org/10.1007/s11207-009-9487-6